Journal of Nanoparticle Research (2005) 7: 489–498
DOI 10.1007/s11051-005-7529-z

Synthesis of iron(III)-doped titania nanoparticles and its application for photodegradation of sulforhodamine-B pollutant

Amar Kumbhar and George Chumanov*
*Department of Chemistry, Clemson University, Clemson, SC, 29634, USA; *Author for correspondence (E-mail: gchumak@clemson.edu)*

Received 28 April 2005; accepted in revised form 3 May 2005

Key words: iron(III)-doped titania, photocatalysis, sol-gel, sulforhodamine-B, titania, visible light, nanotechnology, water quality

Abstract

Iron(III)-doped titania nanoparticles were prepared by modified sol-gel method using titanium (IV) butoxide and inorganic precursor iron(III) nitrate nonahydrate. Spectroscopic measurements show the onset of the band-gap transition to be red-shifted ($\sim\lambda$ = 475 nm) to the visible region with increasing iron(III) ion content. Characterizations were preformed by X-ray diffractometry, electron microscopy, energy dispersive X-ray spectroscopy and X-ray photoelectron spectroscopy. Photocatalysis experiments were performed with dye pollutant sulforhodamine-B in aqueous environment. Direct photocatalytic effect was observed in the dye degradation experiments when irradiated with visible light into the band gap of the iron(III)-doped titania.

Introduction

Amongst semiconductors, the anatase form of titania is known for its high photoactivity and its high photostability. Due to its non-toxic nature and high chemical stability, anatase titania is the most practical semiconductor of choice for various environmental clean-up applications such as water purification and wastewater treatment (Fox & Dulay, 1993; Kamat, 1993; Hoffmann et al., 1995; Linsebigler et al., 1995; Mills & LeHunte, 1997; Fujishima et al., 2000). However, anatase titania has a wide band gap of 3.2 eV and requires UV light (λ < 380 nm) for its activation, so less than 5% of the total solar energy is utilized. Much effort have been focused on sensitizing titania to shift its band gap transition to the visible spectral region, which would allow efficient utilization of solar energy and, hence, would greatly expand its environmental application. Methods such as dye sensitization (Grätzel, 2001, 2003) with molecular chromophores for electrochemical solar cells and doping with non-metal atoms (Asahi et al., 2001; Khan et al., 2002; Ohno et al., 2003; Sakthivel & Kisch, 2003; Gole et al., 2004; Yin & Zhao, 2004) as well as metal ions (Choi et al., 1994; Klosek & Raftery, 2001; Anpo & Takeuchi, 2003; Li et al., 2003) are being explored to extend the photoresponse of titania in the visible region. Metal ion doping is one of the promising ways of shifting the band gap of titania by changing its electronic properties through the formation of "shallow traps" within the titania matrix (Choi et al., 1994). The metal ion dopants alter the intrinsic properties of titania and act as electron or hole traps that increase the photoinduced electron/hole charge recombination lifetimes and in turn the efficiency of its photocatalytic activity (Choi et al., 1994). Among various metal ions, doping with iron(III) has been widely investigated because of its unique

electronic structure and its size that closely matches that of titanium (IV). The energy level of the Fe^{4+}/Fe^{3+} couple is just above the titania conduction band and the energy level of the Fe^{3+}/Fe^{2+} couple is just above the valance band (Choi et al., 1994; Litter & Navio, 1996; Ranjit & Viswanathan, 1997). This favorable electronic states of iron ions in titania leads to formation of efficient trapping sites for electrons and holes.

Iron(III)-doped titania photocatalyst have been synthesized by various techniques such as wet impregnation (Litter & Navio, 1996; Ranjit & Viswanathan, 1997), chemical coprecipitation (Ranjit & Viswanathan, 1997), and sol-gel chemistry (Fuerte et al., 2001; Lopez et al., 2002; Li et al., 2003; Piera et al., 2003; Wang et al., 2003, 2004; Janes et al., 2004). The spectroscopic, structural and photocatalytic properties of various preparations depend on the synthetic procedure and post processing conditions. The optimal dopant concentration that maximizes the photocatalytic activity depends on a specific synthetic method. For a particular synthesis method, optimum dopant concentration directly affect the photoresponse and the photocatalytic activity, however beyond these concentration limits the electronic properties do not relate to the photocatalytic activity due to the formation of surface bound iron oxide phases which may act as recombination sites for the electron/hole pairs (Li et al., 2003).

Here, sol-gel method under constant sonication was employed to prepare iron(III)-doped titania photocatalyst. The photocatalyst were characterized by UV–Vis spectroscopy, X-ray diffractometry, Electron Microscopy, Energy Dispersive X-ray spectroscopy, X-ray photoelectron spectroscopy and tested for its photocatalytic activity in the visible spectral range.

Most dye pollutants pose threat to the environment and are resistant to biodegradation. Dye molecules have high solubility in water and effluents discharged from textile and dye manufacturing industries have adverse effects on the aquatic life and are hazardous to human health. Remediation methods based on physical adsorption of dye molecules on porous media substantially reduce the problem but do not totally eliminate it. There is a growing demand to find effective and inexpensive methods to degrade dye pollutants into non-toxic compounds. Advanced Oxidation Technologies (AOT) (Kamat & Meisel, 2002; Stylidi et al., 2003), utilizing high oxidation potential of hydroxyl radicals generated from light induced semiconductors such as titania, is a complementary approach to degrade or completely mineralize dye contaminants. The UV photogenerated electron-hole pairs interact with the surrounding oxygen (O_2, H_2O) to form highly reactive $O_2^{-\bullet}$, $HOO^{\bullet}$, and $OH^{\bullet}$ radicals, which are strong oxidants (Qua et al., 1998; Liu & Zhao, 2000; Liu et al., 2000a, b; Chen et al., 2002a, b; Stylidi et al., 2003). These radicals can mineralize the dye molecule into water, carbon dioxide and other non-toxic products and the efficiency of this process depends on the extended lifetime of the photogenerated electron-hole pair. Visible light sensitized dye/titania systems have also been known to efficiently degrade dye molecules (Qua et al., 1998; Liu & Zhao, 2000; Liu et al., 2000a, b; Chen et al., 2002b). In this case the pollutant dye molecules act as sensitizers and their complete destruction is a self-limiting process. The mechanism involves excitation of the dye molecules, transfer of electrons from their excited state to the conduction band of titania, resulting in the formation of cationic dye radicals. The injected electrons in the conduction band are responsible for the formation of the reactive radicals in the presence of chemisorbed oxygen. These radicals interact with the cationic dye radical to form lower molecular weight intermediates. The overall efficiency of the process is determined by several steps of electron transfer and migration of electrons to the surface of titania. Because the reaction is self-limiting, complete mineralization of the pollutant is not achieved and further methods including direct UV activation of titania have to be employed for destruction of the intermediate products (Liu & Zhao, 2000). In the current work, we used iron(III)-doped titania catalyst that can be activated by visible light to degrade sulforhodamine-B dye (Figure 1) pollutant with an ultimate goal in applying this technology for water purification.

Experimental section

Materials

Titanium (IV) *n*-butoxide was purchased from Acros Organics. Iron(III) nitrate nonahydrate

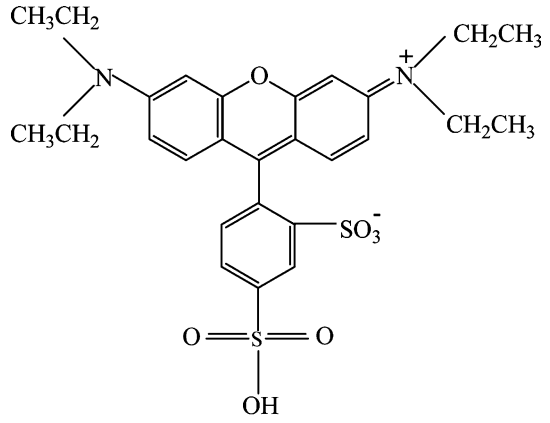

Sulforhodamine-B

Figure 1. Structure of sulforhodamine-B.

($Fe(NO_3)_3{\cdot}9H_2O$) and ethanol was purchased from Fisher Scientific. All chemicals were used without any further purification. Millipore pure (>18 MΩ) from our in-house system was used throughout the synthesis.

Synthesis of undoped and doped titania

Iron(III)-doped titania photocatalyst were synthesized by a modified sol-gel process under constant sonication. In a typical synthesis, 200 μl of titanium (IV) *n*-butoxide alkoxide precursor in 15 ml ethanol is allowed to undergo hydrolysis at room temperature in the presence of 1 ml of water. The resulting solution immediately turns white indicating the formation of hydrolyzed titania particles. Certain amount of ethanolic solution of an inorganic precursor $Fe(NO_3)_3{\cdot}9H_2O$ (typically 1% solution) was added to the hydrolyzed titania solution under constant sonication. The reaction mixture is allowed to proceed to condensation under sonication for 30 min. As the concentration of the $Fe(NO_3)_3{\cdot}9H_2O$ is increased, the color of the reaction mixture changes from a milky yellow to dark milky brown. Undoped titania was prepared by the same procedure without the addition of $Fe(NO_3)_3{\cdot}9H_2O$. The overall amount of water and ethanol is kept constant for both undoped titania and doped titania reactions. No additional effort was made to control the pH of the reaction mixture. The sample were denoted as TiO_2 for undoped titania and TFe0.5, TFe1, TFe1.5, TFe2 for the samples prepared by adding 0.5, 1, 1.5, and 2 ml of 1% ethanolic $Fe(NO_3)_3{\cdot}9H_2O$ solution. Further, the precipitate was washed with ethanol and centrifuged several times to remove excess Fe^{3+}, NO_3^- and water present in the reaction. The precipitate was allowed to dry overnight at 100°C to remove organics used during the synthesis and then heat treated in a crucible for 5 h to convert the amorphous titania into the crystalline anatase form. The temperature was kept at 450°C to avoid the formation of rutile phase. The heat-treated samples do not lose their color after sonication in aqueous or ethanolic solutions and the filtration leaves clear filtrate indicating absence of leaching of the iron(III) ions. The samples were ground into a fine powder and were kept in the oven set at 100°C for further characterization.

UV–Vis absorption spectra

UV–Vis absorption spectra were recorded on Shimadzu UV-2501PC Spectrophotometer. Spectra were obtained by diluting 10 μl of the sample to 2 ml in ethanol. All the spectra were obtained at room temperature and processed using Origin® 7SR2 software (OriginLab Corporation).

X-ray powder diffraction

X-ray powder diffraction (XRD) analysis was performed on SCINTAG XDS 2000 using Cu–Kα radiation ($\lambda = 1.5418$ Å). The diffraction patterns were recorded at room temperature.

Scanning transmission electron microscopy

The morphology of the doped and undoped titania nanoparticles was observed with HITACHI HD2000 Scanning Transmission Electron Microscope (STEM) equipped with an Energy Dispersive X-ray detector (EDX). The samples were prepared by evaporating a drop of the sample on a carbon-coated copper grid (Ted Pella, Inc.). All images were obtained in the SEM mode with the emmision gun operated at 200 kV acceleration voltage.

X-ray photoelectron spectroscopy

X-ray photoelectron spectroscopy (XPS) analysis were performed with a monochromatic Al–Kα source on a Kratos Analytical AXIS 165 system

equipped with a charge neutralizer. Binding energies were referenced to C1s peak at 284.8 eV. Spectra were processed using VISION data system.

Photocatalytic activity

The photocatalytic activity of the iron(III)-doped titania nanoparticles was evaluated by the decolorization of sulforhodamine-B (SRB) (Aldrich, laser grade). The dye concentration was maintained at 10^{-7} M for all the photocatalytic reactions. The photocatalytic measurements were performed in a 50 ml pyrex photoreactor at room temperature and atmospheric pressure in a dark room. The reactor was placed at a fixed distance of 10 cm from the lamp housing. A 150 W Xe lamp was employed as a visible light source. UV cutoff filter was placed between the irradiation source and the photoreactor to eliminate radiation below 420 nm. The aqueous solutions of SRB (typically 15 ml) and 5 mg of the catalyst were sonicated in a pyrex photoreactor for half an hour before irradiation. The solutions were constantly stirred with a magnetic stirrer during the photocatalytic experiments. At regular intervals, 1 ml of samples were collected, centrifuged to remove all the photocatalyst and 500 μl aliquots of the filtrate was diluted to 2 ml in water and were analyzed for decoloration by UV–Vis spectroscopy at its characteristic absorption band at 565 nm.

Results and discussion

UV–Vis absorption spectra of the as prepared titania and iron(III)-doped titania with increasing amounts of iron content before heat treatment is presented in Figure 2. It can be seen that the iron(III)-doped titania samples show a relatively sharp band-gap transition typical of semiconductors and does not show any absorption characteristic of isolated iron oxide phases in the visible region. Even at a low concentration of $Fe(NO_3)_3 \cdot 9H_2O$ (0.5 ml), the onset of the band-gap transition was already red shifted to 435 nm as compared to 360 nm for undoped TiO_2. The shift is consistent with the incorporation of iron(III) ions into the titania matrix and also possibly due to the presence of iron oxide bound to the surface of the titania, although the contribution from the later is not expected to be significant. The red shift is attributed to the transfer of 3d-electrons from the iron(III) ions to the conduction band (Hoffmann et al., 1995; Ranjit & Viswanathan, 1997). An

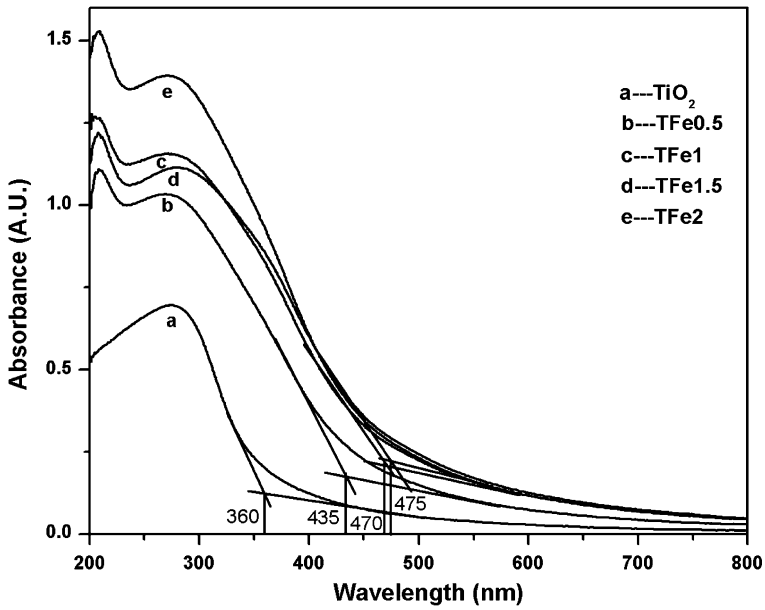

Figure 2. UV–Vis absorption spectra of undoped titania and iron(III)-doped titania nanoparticles with increasing amounts of 1% ethanolic $Fe(NO_3)_3 \cdot 9H_2O$ solution.

increase of $Fe(NO_3)_3 \cdot 9H_2O$ to 1.5 ml in the reaction mixture leads to 475 nm red shift of the band-gap absorption onset. However, any further increase of iron does not induce more red shift indicating the presence of an optimum doping level. Instead of the red shift of the band gap, high concentration of $Fe(NO_3)_3 \cdot 9H_2O$ affect the condensation step leading to the reaction mixture becoming progressively transparent. This brown and transparent solution consists of small hydrolyzed titania particles and iron hydroxide. After drying and heat treatment the re-suspended material does not exhibit any photocatalytic activity with visible light.

The XRD pattern (Figure 3) of the samples heat-treated at 450°C for 5 h indicate the presence of smaller size nanoparticles in both TiO_2 and TFe1.5 samples. The broad characteristic (101), (200) and (105) diffraction peaks of mesoporous anatase TiO_2 can be clearly seen. The diffraction pattern of TFe1.5 shifts to higher 2 theta angles suggesting the incorporation of iron(III) ions and substitution of the tetravalent titanium ions with the trivalent iron ions resulting in some lattice distortion. Similar results were observed for TiO_2 doped with chromium ion (Kudo & Kato, 2002; Ma et al., 2004). The diffraction pattern of TFe1.5 follows that of TiO_2 suggesting that no phase transition took place at this doping level. Typical SEM micrographs for TiO_2 and TFe1.5 samples are presented in Figure 4. The as prepared TiO_2 and TFe1.5 (Figure 4a and c) are amorphous forming aggregates less than 50 nm in size. These aggregates are composed of small, less than 5 nm amorphous titania nanoparticles (Kumbhar & Chumanov, 2004). In contrast, the heat-treated samples of TiO_2 appear to be crystalline (Figure 4b). The small amorphous titania particles fuse for form ca. 50 nm mesoporous agglomerated particles. The presence of iron(III) ions in the doped samples seems to have some effect on their crystallization. The SEM images of the doped samples resemble those before the heat treatment (Figure 4d) and the presence of 100 nm spherical agglomerates of small particles are apparent. Conceivably, incorporation of iron(III) ions leads to lattice distortion and the presence of iron-oxygen species on the surface of the doped titania nanoparticles results in the formation of large aggregates when treated at 450°C.

EDX spectroscopy was employed to determine the distribution of iron in the titania matrix. This

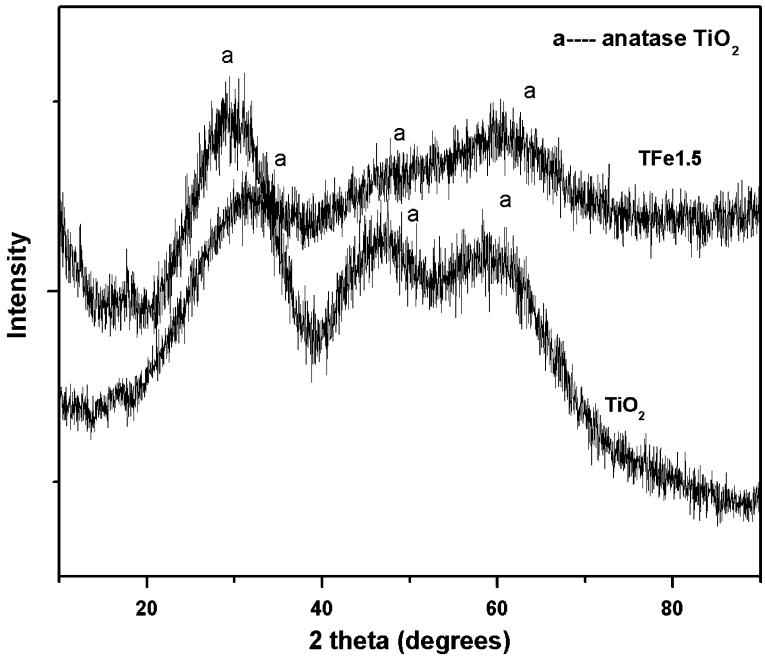

Figure 3. XRD powder diffraction pattern for TiO_2 and TFe1.5 nanoparticles after 5 h of heat treatment at 450°C.

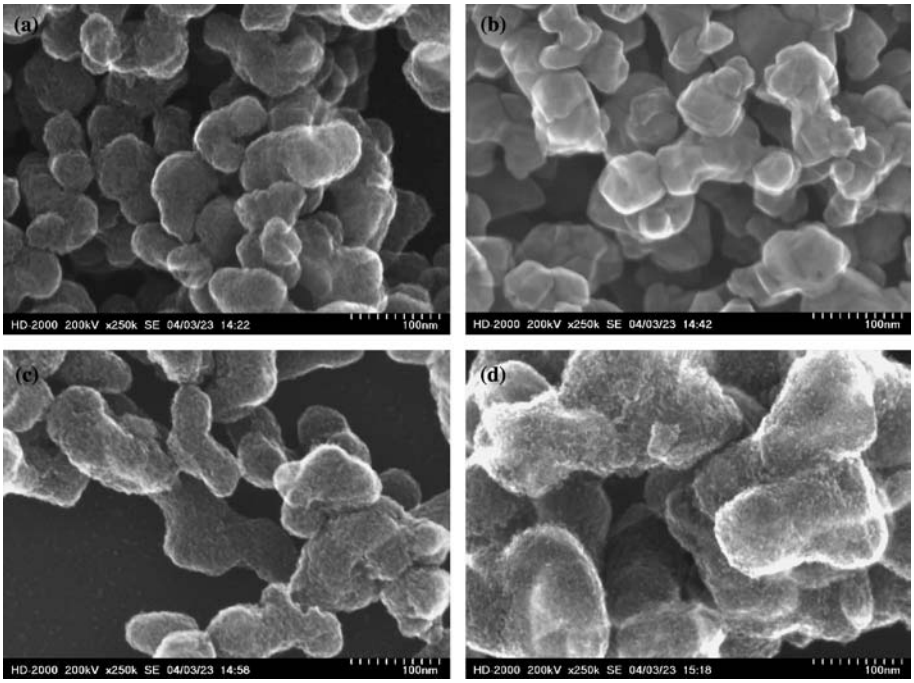

Figure 4. SEM images of (a) as prepared TiO_2 (b) heat-treated TiO_2 (c) as prepared TFe1.5 (d) heat-treated TFe1.5 nanoparticles.

technique is a site specific quantitative technique and averaging over several cross section of several particles gave average iron content of 8 atomic %. A representative EDX spectrum is presented in Figure 5. Typical EDX mapping scans (Figure 6) suggests the uniform distribution of iron within the titania matrix indicating no phase segregation occurs during the synthesis and post treatment procedures.

XPS analysis was performed on the undoped and doped catalysts to confirm the valence state of titanium and iron. Figure 7 shows the representative survey scans for heat treated TiO_2 and TFe1.5. It is noted that the doped titania samples

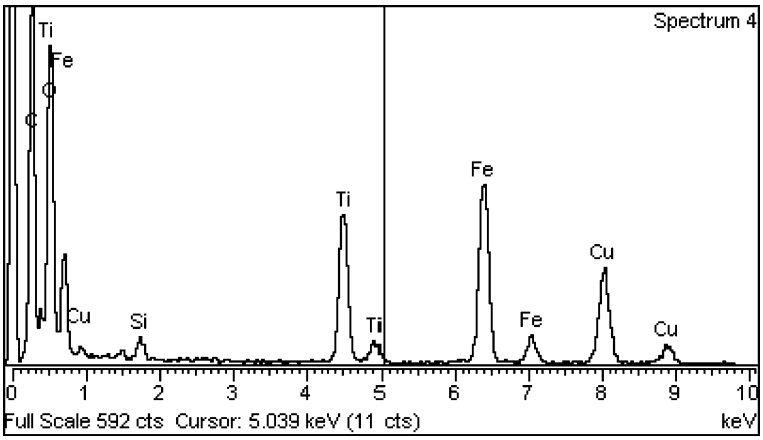

Figure 5. Energy Dispersive X-ray spectra of TFe1.5 nanoparticles.

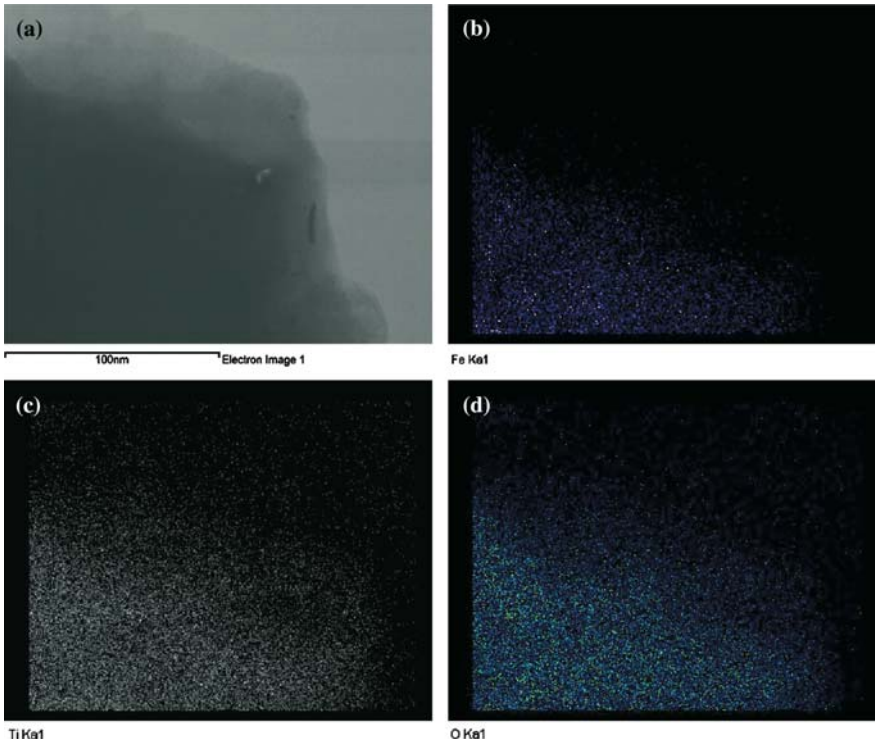

Figure 6. Energy Dispersive X-ray mapping image of TFe1.5 (a) TEM image (b) Fe (c) Ti (d) Oxygen mapping scans.

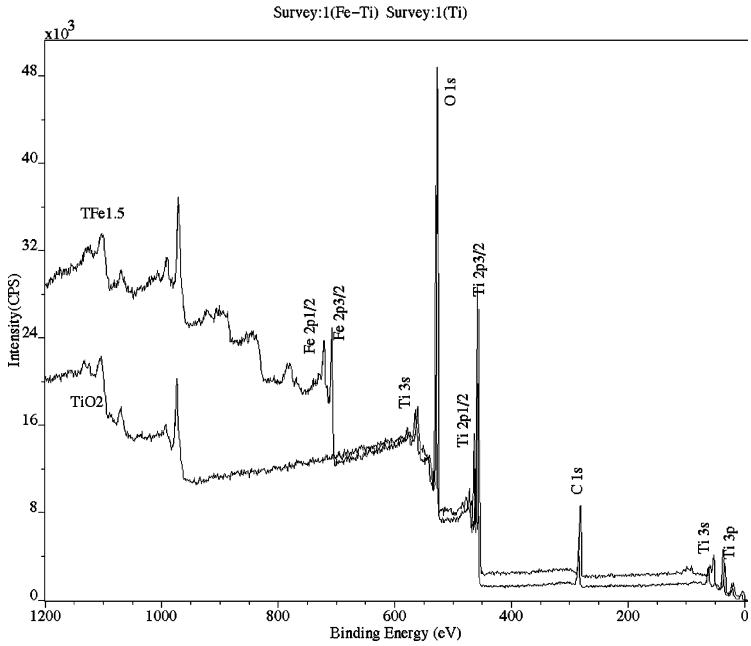

Figure 7. Survey scans for TiO_2 and TFe1.5.

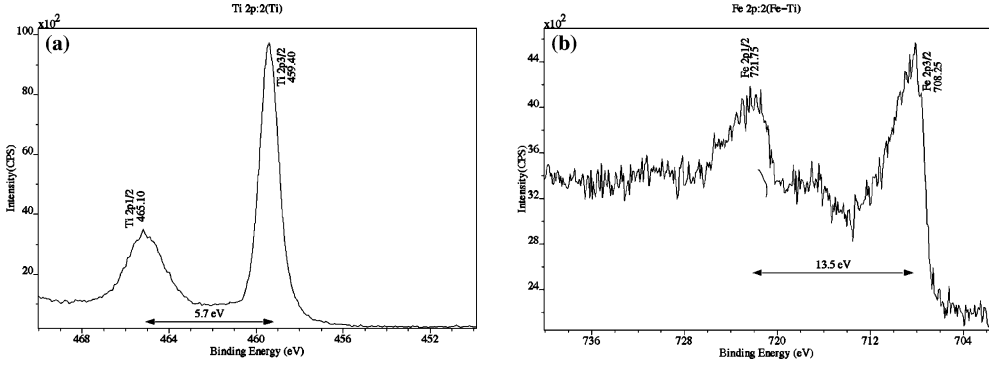

Figure 8. High resolution scans of (a) Ti 2p and (b) Fe 2p regions.

contain peaks of Ti, O, Fe and a trace amount of carbon. Ti $2p_{3/2}$ and Ti $2p_{1/2}$ peaks appear at 459.4 eV and 465.10 eV and Fe $2p_{3/2}$ and Fe $2p_{1/2}$ peaks appear at 708.25 eV and 721.75 eV respectively. The peak corresponding to O 1 s appears at 530.5 eV, and is typical for metal oxides. High resolution scan shows splitting of 5.7 eV in Ti $2p_{1/2}$ and Ti $2p_{3/2}$ peaks (Figure 8a), suggesting the presence of titanium in its tetravalent state which is consistent with the formation of TiO_2. 13.5 eV separation in Fe $2p_{1/2}$ and Fe $2p_{3/2}$ (Figure 8b) peaks reveals the presence of iron in its trivalent state (Moulder et al., 1995).

It is known that SRB undergoes direct photocatalysis under UV irradiation and photosensitization when illuminated with visible light (Qua et al., 1998; Liu & Zhao, 2000; Liu et al., 2000a, b; Chen et al., 2002b). The mechanisms under both modes of irradiation have been extensively studied and can be represented by the following reactions (Qua et al., 1998; Stylidi et al., 2003).

Direct photocatalysis under UV irradiation:

$$TiO_2 + h\nu(UV) \rightarrow h^+(vb) + e^-(cb)$$

$$SRB(adsorbed) + h^+(vb) \rightarrow SRB^{\bullet}(adsorbed)$$

$$H_2O/O_2 + h^+(vb) \rightarrow {}^{\bullet}OH + H^+$$

$$OH^-(adsorbed) + h^+(vb) \rightarrow {}^{\bullet}OH(adsorbed)$$

$$O_2(adsorbed) + e^-(cb) \rightarrow O_2^-(adsorbed)$$

$$SRB^{\bullet}(adsorbed) + ({}^{\bullet}OH, O_2^-) \rightarrow Mineralized\ products(CO_2 + H_2O + SO_4^{2-} + NH_4^+)$$

Photosensitization when illuminated with visible light:

$$SRB(adsorbed) + h\nu(Visible) \rightarrow SRB^*(adsorbed)$$

$$SRB^*(adsorbed) + TiO_2 \rightarrow TiO_2(e^-(cb)) + SRB^+(adsorbed)$$

$$O_2(adsorbed) + TiO_2(e^-(cb)) \rightarrow O_2^{\bullet}(adsorbed)$$

$$SRB^*(adsorbed) + O_2(adsorbed) \rightarrow SRB^+(adsorbed) + O_2^-(adsorbed)$$

$$SRB^+(adsorbed) + (O_2^-) \rightarrow (degraded\ intermediates)$$

$$(degraded\ intermediates) + h^+(vb)\ or\ {}^{\bullet}OH \rightarrow Mineralized\ products(direct\ photocatalysis)$$

The intermediates formed during photosensitization have to undergo an additional direct photocatalysis step to be mineralized. The difference in the mechanism has been associated to the formation of active oxygen radicals $\{O_2^{\bullet}$ (adsorbed)$\}$ (Liu & Zhao, 2000), which plays an important role in the disintegration pathway of the chromophore structure.

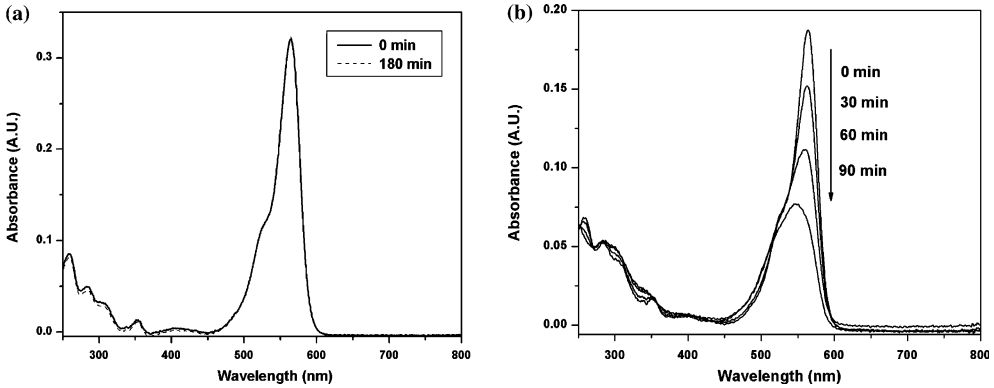

Figure 9. UV–Vis absorption spectra of aqueous solution of sulforhodamine-B (a) in the presence of TiO_2 and (b) in the presence of TFe1.5 during visible light illumination.

No oxidation of SRB was observed in the presence of undoped titania irradiated with visible light above 420 nm despite the fact that the rapid oxidation was noted when the same mixture was irradiated with UV light (Figure 9a). Even after 3 h of visible light irradiation using 150 W Xe lamp, there is no effect on the intensity of the characteristic absorption peak of SRB. Lack of oxidation under visible irradiation indicates that sensitization did not occur and can be reasoned by specific experimental conditions employed. Similar observation was seen in the photocatalytic experiments of aqueous solutions of SRB in the presence of Degussa P25 under the same experimental conditions. When doped titania and SRB were irradiated with visible light a well-pronounced oxidation of the dye was evident from the sharp decrease of the intensity and slight blue shift of the absorption maximum at 565 nm (Figure 9b). It is important to emphasize that SRB undergoes photobleaching as indicated by the rapid decrease of the absorbance at its maximum with no additional absorbance increase elsewhere. This mechanism is consistent with that proposed for direct photocatalysis under UV irradiation of undoped titania (Liu & Zhao, 2000), thereby supporting the conclusion that, in the case of iron doping, the photocatalysis results from band-gap excitation and not from sensitization of the dye. Because no additional absorbance peaks were observed elsewhere in the spectrum during the photodegradation with iron doped titania, no other intermediates where formed and no additional steps for their remediation is required.

Conclusions

Iron(III)-doped titania is stable, inexpensive photocatalyst with activation in the visible spectral range that can be used for water purification applications. Tests with a dye pollutant sulforhodamine-B revealed direct band-gap photodegradation as the main mechanism for its mineralization. Because the destruction of the dye took place in one step, no additional remediation techniques are required to further degrade intermediates that are formed when photosensitization methods are employed.

Acknowledgments

We gratefully acknowledge the support of this work through EPA Grant No. STAR R-82960301. We also acknowledge Julie Cooper for help in ICP-AES analysis and Mr. Bill Kay for help in XPS analysis.

References

Anpo M. & M. Takeuchi, 2003. J. Catal. 216, 505–216.
Asahi R., T. Morikawa, T. Ohwaki, K. Aoki & Y. Taga, 2001. Science 293(5528), 269–271.
Chen C., W. Zhao, J. Li, J. Zhao, H. Hidaka & N. Serpone, 2002. Environ. Sci. Technol. 36(16), 3604–3611.
Chen C., X. Li, W. Ma, J. Zhao, H. Hidaka & N. Serpone, 2002. J. Phys. Chem. B 106(2), 318–224.
Choi W., A. Termin & M.R. Hoffmann, 1994. J. Phys. Chem. B. 98, 13669–13679.

Fox M.A. & M. Dulay, 1993. Heterogen. Photocatal. Chem. Rev. 93, 341–357.
Fuerte A., M.D. Hernandez-Alonso, A.J. Maira, A. Martinez-Arias, M. Fernandez-Garcia, J.C. Conesa & J. Soria, 2001. Chem. Commun. 2718–2719.
Fujishima A., T.N. Rao & D. Tyrk, 2000. J. Photochem. Photobiol. C: Photochem. Rev. 1, 1–21.
Gole J.L., J.D. Stout, C. Burda, Y. Lou & X. Chen, 2004. J. Phys. Chem. B 108(4), 1230–1240.
Grätzel M., 2001. Nature 414, 338–344.
Grätzel M., 2003. J. Photochem. Photobiol., C: Photochem. Rev. 4(2), 145–153.
Hoffmann M.R., S.T. Martin, W. Choi & D.W. Bahnemann, 1995. Chem. Rev. 95, 69–96.
Janes R., L.J. Knightley & C.J. Harding, 2004. Dyes Pigments 62(3), 199–212.
Kamat P.V., 1993. Chem. Rev. 93, 267–300.
Kamat P.V. & D. Meisel, 2002. Curr. Op. Coll. Inter. Sci. 7, 282–287.
Khan S.U.M., M. Al-Shahry & W.B. Ingler Jr., 2002. Science 297(5590), 2243–2245.
Klosek S. & D. Raftery, 2001. J. Phys. Chem. B 105, 2815–2819.
Kudo A. & H. Kato, 2002. J. Phys. Chem. B 106, 5029–5034.
Kumbhar A. & G. Chumanov, 2004. J. NanoSci. NanoTech. 4(3), 299–303.
Li W., Y. Wang, H. Lin, S.I. Shah, C.P. Huang, D.J. Doren Rykov, A. Sergey, J.G. Chen & M.A. Barteau, 2003. Appl. Phys. Lett. 83(20), 4143–4145.
Li X., P.-L. Yue & C. Kutal, 2003. N. J. Chem. 27(8), 1264–1269.
Linsebigler A.L., G. Lu & J.T. Yates, 1995. Chem. Rev. 95, 735–758.
Litter M.I. & J.A. Navio, 1996. J. Photochem. Photobiol. A 98, 171–181.
Liu G., J. Zhao & H. Hidaka, 2000. J. Photochem. Photobiol. A 133(1-2), 83–28.
Liu G., X. Li, J. Zhao, H. Hidaka & N. Serpone, 2000. Environ. Sci. Technol. 34(18), 3982–3990.
Liu G. & J. Zhao, 2000. N. J. Chem. 24(6), 411–417.
Lopez T., J.A. Moreno, R. Gomez, X. Bokhimi, J.A. Wang, H. Yee-Madeira, G. Pecchi & P. Reyes, 2002. J. Mater. Chem. 12(3), 714–718.
Ma W., C. Chen, J. Zhao, Z. Shuai & W. Zhao, 2004. J. Am. Chem. Soc. 126, 4782–4783.
Mills A. & S. LeHunte, 1997. J. Photochem. Photobiol. A: Chem. 108, 1–35.
Moulder, J.F., W.F. Stickle, P.E. Sobol & K.D. Bomben, 1995. Handbook of X-ray Photoelectron Spectroscopy. Physical Electronics.
Ohno T., T. Mitsui & M. Matsumura, 2003. Chem. Lett. 32(4), 364–365.
Piera E., M.I. Tejedor-Tejedor, M.E. Zorn & M.A. Anderson, 2003. Appl. Catal. B. Environ. 46, 671–685.
Qua P., J. Zhao, T. Shen & H. Hidaka, 1998. J. Mol. Catal. A 129, 257–268.
Ranjit K.T. & B. Viswanathan, 1997. J. Photochem. Photobio. A 108, 79–84.
Sakthivel S. & H. Kisch, 2003. Angew. Chem. Int. Ed. 42, 4908–4911.
Stylidi M., D.I. Kondarides & X.E. Verykios, 2003. Appl. Catal. B. Environ. 40, 271–286.
Wang C., Q. Li & R. Wang, 2004. J. Mater. Sci. 39(5), 1899–1901.
Wang C.-Y., C. Boettcher, D.W. Bahnemann & J.K. Dohrmann, 2003. J. Mater. Chem. 13(9), 2322–2329.
Yin J.B. & X. Zhao, 2004. Chem. Mater. 16, 321–328.